ORIGINAL ARTICLE

Assessment of Morphological Changes in Breast Cancer Cells Following X-ray Radiation Utilizing Digital Holographic Microscopy

Zeinab Hormozi-Moghaddam [1,2], Seyedeh Mona Taheri [1], Reza paydar [1,2], Ali Neshasteh-Riz [1,2*], Vahideh Farzam Rad [3], Mohadeseh Shaghaghi [3]

[1] *Radiation Biology Research Center, Iran University of Medical Sciences, Tehran, Iran.*

[2] *Radiation Sciences Department, Iran University of Medical Sciences, Tehran, Iran.*

[3] *Department of Physics, Institute for Advanced Studies in Basic Sciences, Zanjan, Iran*

*Corresponding Author: Ali Neshasteh-Riz
Email: Neshastehriz@yahoo.com

Received: 16 November 2023 / Accepted: 03 March 2024

Abstract

Purpose: Digital holographic microscopy, being a label-free and entirely non-invasive technique, proficiently facilitates the quantitative assessment of morphological alterations in living cells. The primary objective of this investigation is to scrutinize the capability of a digital holographic microscope in assessing the morphological transformations of cancer cells exposed to X-ray radiation.

Materials and Methods: The Michigan Cancer Foundation-7 (MCF7) cell line underwent exposure to X-ray radiation, administered in a singular fraction at a dose of 2 Gy. Subsequently, the MCF7 cell group was subjected to imaging through a digital holographic microscope. To scrutinize the morphological alterations between the radiation-exposed and control groups, the pertinent image parameters were extracted through the three-dimensional reconstruction of the microscopic images.

Results: The results indicate a significant increase in the morphological parameters of cells, encompassing volume, and roughness, subsequent to radiation exposure when contrasted with the control group. This observation signifies discernible alterations in the shape and roughness characteristics of MCF7 cells.

Conclusion: By extracting various parameters and broadening the spectrum of morphological and physical attributes, it becomes feasible to establish a more precise correlation between cellular conditions and the response to treatment. Such investigations pave the way for a more intricate exploration of cell morphology, enabling the identification of more specific parameters and distinctions in cellular response.

Keywords: Digital Holographic Microscopy; Morphological Parameters; Radiation; Michigan Cancer Foundation-7 Cells.

DOI:

1. Introduction

Radiotherapy stands as a pivotal and predominant modality for the management of malignant tumors, catering to the treatment needs of over 60% of individuals afflicted with cancer [1]. In recent decades, there has been a rapid evolution in radiotherapy technology, which has made significant advances aimed at increasing treatment accuracy, accelerating treatment processes, and simultaneously reducing adverse side effects [2, 3]. In conjunction with these technological advances, the expanding reservoir of knowledge in the fields of biology, immunology, physiology, and radiobiology enables the implementation of radiation therapy with greater effectiveness [4]. Numerous investigations have elucidated the intricate interplay between cellular functionalities, such as cell growth [5], intercellular connections [6], transcriptome, and proteome [7], with morphological phenotypes. The configuration of a cell is intricately related to its diverse functions and activities. Ionizing radiation can affect biological function, as evidenced by changes in the dimensions of living cells attributed to processes such as cell proliferation or cell death. Furthermore, the survival status of cells can be reasonably inferred through careful observation of cell morphology. The final fate of a cell after radiation exposure consistently corresponds to some recognizable morphological manifestation [8]. Consequently, morphological parameters emerge as a pivotal source of essential information for the assessment and inference of cellular physiological states, particularly in gauging cellular responses to external stimuli such as radiation [9, 10]. In phase imaging techniques, the temporal delay induced by the passage of light through the imaged cells, due to the higher refractive index of the cells compared to their surrounding environment, is used to create contrast. However, conventional intensity-based detectors lack the speed required to capture this light delay directly [11]. Enter Digital Holographic Microscopy (DHM) and use phase imaging techniques. DHM combines the advantages of optical microscopy and digital holography with the capability of quantitative phase microscopy imaging [12]. This technique has been widely used in recent years to evaluate morphological changes and monitor cell growth, viability, and destruction. Unlike methods such as Western blotting and staining methods that measure the release of extracellular markers, the main feature of DHM is its ability to capture images without any physical contact or sample manipulation, making it particularly suitable for examining fragile or sensitive samples such as cells. or live tissues [13-20]. The versatility of DHM is evident in its diverse applications, and in the field of biomedical research, DHM is effective in real-time investigation of living cells and tissues and provides valuable insights into their dynamic behavior and function [21]. Notably, DHM dispenses with the necessity for intricate scanning configurations, presenting a straightforward setup [22]. Numerous statistical metrics are available for the evaluation of holographic quality and the signal-to-noise ratio in the reconstructed image. Within the DHM methodology, parameters such as Volume, Standard Deviation (STD), Kurtosis, and Skewness are computed for the intensity distribution of a hologram. These metrics serve not only as evaluative tools for holographic assessments but can also be employed for comparative analyses of distinct samples or conditions. Additionally, they prove valuable in monitoring temporal alterations in the size or shape of a specimen over time [23].

This novel approach is anticipated to exert a profound influence on cell morphology-focused research, offering a platform for a more intricate examination of cell morphology and fate without the need for labeling [23-26]. Recently, the use of DHM in identifying changes in cell morphology after radiation has attracted attention [27, 28]. As in the previous study, morphological changes of irradiated bladder cancer cells were observed using DHM [29]. Despite the importance of morphological aspects, unfortunately, so far, most studies have focused on molecular aspects. However, expanding the understanding of the morphological changes after receiving radiation can certainly help to improve the clinical view and predict the response to the treatment of cancer cells. There is a gap in a study on the observation and identification of morphological changes in breast cancer cells caused by radiation using DHM, like what has been done on bladder cancer. Therefore, in the present study, the aim is to investigate and identify the morphological changes of breast cancer cells (MCF7) cells pre- and post-radiation exposure, with the help of real-time cell observation by DHM. In essence, DHM emerges as a potent tool for comprehensively exploring morphological transformations in MCF7 cells, thereby aiding researchers in gaining a deeper understanding of the mechanisms involved in cancer treatment and facilitating the development of more efficacious therapeutic strategies. Within this study, we delve into the

morphological changes exhibited by unstained and living MCF7 cells subjected to radiation.

2. Materials and Methods

2.1. Cell Culture

In this investigation, the MCF7 cell line underwent cultivation in DMEM medium supplemented with 10% FBS and 1% streptomycin. The cells were maintained in an incubator set at 37°C with 5% carbon dioxide and 95% humidity until reaching passage 4. Subsequently, viable cells were enumerated, and 3 cm Petri dishes were employed for seeding, with a density of 10×10^5 cells. The cells were subsequently allocated into two distinct groups: the control group (Ctrl) and the group exposed to 2 Gy X-ray radiation (Radiation). Each group underwent five replicates for comprehensive analysis.

2.2. Radiation

The irradiation of MCF7 cells was conducted utilizing a 6 MeV linear accelerator (Electa compact, single energy) at Firouzgar Hospital, affiliated with Iran University of Medical Sciences. The irradiation parameters were configured based on a field size of 30x30 cm square, and the source-to-surface distance (SSD) was set at 100 cm. A single radiation dose of 2 Gy was administered, with specific settings of 169 monitor units (MU) and a gantry rotation of 180 degrees according to the treatment planning system (Figure 1). To facilitate uniform scattering, a 3 cm thick Perspex was positioned below the plate, accompanied by a thin moistened towel, while an additional 3 cm Perspex was placed above the plate.

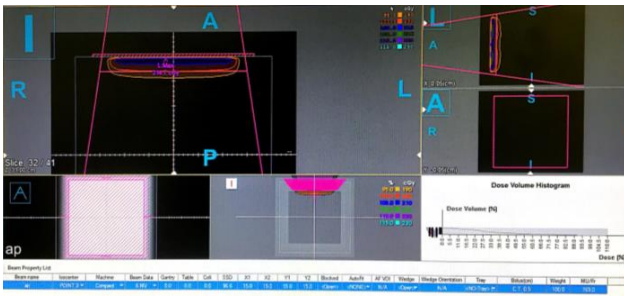

Figure 1. Radiation plan prepared by CorePLAN treatment planning system

2.3. Digital Holographic Microscopy (DHM) Protocol

MCF7 cells were cultured in a confocal dish and incubated at 37°C with 5% CO_2 one day before imaging. During the imaging process, each dish was subdivided into multiple sections, with each section undergoing imaging procedures on three separate occasions.

2.3.1. Experimental Setup

Figure 2 schematically illustrates the DHM setup employed in this research, utilizing a Mach–Zehnder geometry, which proves to be a suitable configuration for off-axis holography of transparent specimens. The coherent beam generated by a He–Ne laser (MEOS, 632.8 nm, 5 mW, linearly polarized) is bifurcated into object and reference waves by the initial Beam Splitter (BS1).

As delineated in Figure 2, a laser beam is employed, focusing laser light through an objective lens (MO_1) to a specific focal point. Subsequently, a Beam Expander (BE1) widens the laser beam to encompass the entire sample area. Post-expansion, the laser beam undergoes division into two beams through a Beam Splitter (BS1). One of the beams traverses the sample, while the other, serving as the reference beam, does not. Before reaching the sample, one of the beams encounters mirrors m1 and is then focused onto the sample by a condenser lens (C, NA = 1.25, Olympus). Simultaneously, the other beam, designated as the reference beam, reflects towards an objective (MO_2) via the M2 mirror and subsequently interferes with a beam emerging from the sample through a second Beam Splitter (BS2). The reference beam is directed toward a mirror and then to a CCD camera, whereas the object beam is directed toward the sample under observation. Interaction with the sample induces alterations in the phase and amplitude of the light in the object beam. Subsequently, the object and reference beams reunite at the CCD camera, initiating interference and generating a hologram. This holographic data undergoes processing to reconstruct a three-dimensional image of the sample.

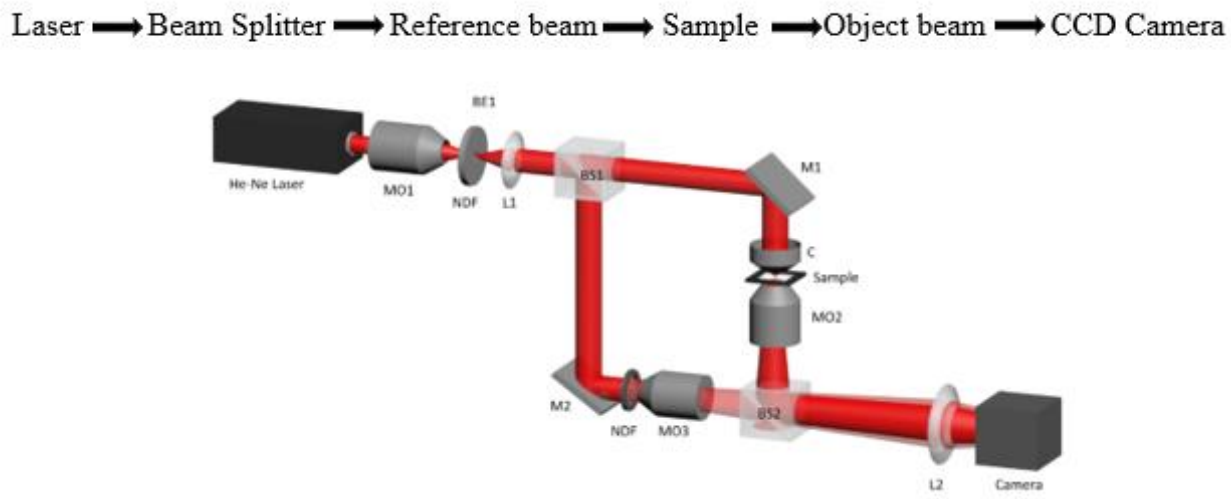

Figure 2. A schematic representation of the experimental DHM setup: BS, beam splitter; M, mirror; NDF, neutral density filter; C, condenser; MO, microscope objective

2.3.2. Image Reconstruction and Analysis

In the classical electrodynamics theory, light is conceptualized as a transverse wave. As it interacts with or reflects off an object, alterations in its phase and amplitude may occur, influenced by the inherent properties of the object (Equation 1). The intricate amplitude of the reflected or transmitted light wave is articulated as follows:

$$E(x,y) = E_0(x,y)e^{i\phi(x,y)} \quad (1)$$

where $E_0(x,y)$ and $\phi(x,y)$ denote the amplitude and phase of the wave, respectively. In instances involving phase objects, it is the phase ϕ that undergoes modification. Phase alterations stem from changes in the optical path length traversed by the reflected or transmitted light, directly correlating with variations in thickness and refractive index in transmission mode or surface height characteristics in reflection mode (Equation 2):

$$\phi(x,y) = \frac{2\pi\, n(x,y)d(x,y)}{\lambda} \quad (2)$$

Here, λ represents the light wavelength, $n(x,y)$ embodies the refractive index distribution, and d(x,y) signifies the physical path difference of the two beams. In scenarios involving reflective objects, where both the reference and object waves propagate in air $n(x,y) = 1$, the phase change relies solely on alterations in physical distance. Upon the interference of a wave with a reference wave, the resulting interference pattern, or the recorded hologram, is transformed (Equation 3):

$$I(x,y) = |E_{0s}(x,y)|^2 + |E_{0r}(x,y)|^2 + E_{0s}(x,y)E_{0r}^*(x,y)e^{i\phi_s}\, e^{-i\phi_r} + E_{0s}^*(x,y)E_{0r}(x,y)e^{-i\phi_s}\, e^{i\phi_r} \quad (3)$$

Here, E_{0s}, ϕ_s, and E_{0r},ϕ_r denote the amplitudes and phases of the object and reference waves, respectively.

In the numerical reconstruction process, the numerical value is illuminated by the same reference wave, propagating through the subsequent numerical space in the image formation. This holistic hologram reconstruction engenders a complex wave image, ultimately yielding a three-dimensional representation of the object's index. In the realm of digital holography, reconstruction employs diverse algorithms, and in this context, we employ the Angular Spectrum Propagation (ASP) approach [30].

The angular spectrum, representing the Fourier transform of the light wave at the hologram plane $E_s(x,y,z=0)$, is acquired through the numerical illumination of the recorded digital hologram by the reference wave (Equation 4):

$$FT\{E_s(x,y)\} = \tilde{E}_s(u,v) \equiv \iint_{-\infty}^{\infty} E_s(x,y,0)\, e^{-2\pi i(ux+vy)}dxdy \quad (4)$$

Here, u and v denote the spatial frequencies in the x and y directions, respectively. In the Fourier domain, the zero term and the conjugate real image are filtered

out. Through an inverse Fourier transform, the modified light wave $\tilde{E}_S^F$ is obtained as (Equation 5):

$$E_s^f(x,y,0) = FT^{-1}\{\tilde{E}_s^F(u,v,0)\} \equiv \iint_{-\infty}^{\infty} \tilde{E}_S^F(u,v,0)e^{2\pi i(ux+vy)}\,dxdy \quad (5)$$

The complex amplitude at an arbitrary plane situated at $z = d$ is determined by free space propagation of $E_s(x,y,0)$ over a distance d, where λ is the wavelength of the laser beam (Equation 6):

$$E_S^F(x,y,d) = \iint_{-\infty}^{\infty} \tilde{E}_S^F(u,v,0)e^{ikd\sqrt{1-\lambda^2u^2-\lambda^2v^2}} \times e^{2\pi i(ux+vy)}dudv \quad (6)$$

The entire process can be succinctly summarized as follows (Equation 7):

$$E_S^F(x,y,d) = FT^{-1}\left\{|FT\{E_S(x,y,0)\}|^F e^{ikd\sqrt{1-\lambda^2u^2-\lambda^2v^2}}\right\} \quad (7)$$

ϕ_s, the phase of the object, and I_S, the intensity of the object, are calculated from the complex amplitude (Equations 8 and 9).

$$\phi_S(x,y,z) = tan^{-1}\frac{\Im[E_S^F(xy,z)]}{\Re[E_S^F(xyz)]} \quad (8)$$

$$I_s(x,y,z) = \left|E_s^f(x,y,z)\right|^2 \quad (9)$$

If deemed necessary, the numerical reconstruction process allows for the implementation of phase and amplitude smoothing. Equation 8 delineates the phase map of an object, encapsulating three-dimensional details pertaining to phase attributes. The phase map is directly proportional to the optical path length, expressed as $\varphi = \frac{2\pi}{\lambda}nL$, wherein n represents the refractive index of the medium, and L is the physical length through which the light beam propagates.

An intensity image, akin to that of a bright-field microscope image, can be derived through equation 9. However, DHM uniquely facilitates numerical focus adjustment. Consequently, rather than mechanically altering the target position, a complex range can be computed for any designated axial plane by adjusting the propagation distance (d in Equation 7), yielding the corresponding intensity image. This study scrutinized morphological transformations, encompassing changes in shape and roughness, employing parameters such as volume, STD, kurtosis, and skewness. The analysis utilized 3D reconstruction via MATLAB software (The MathWorks Inc., Massachusetts, US), with the obtained values presented as the ratio of morphological parameters in the radiation group to those in the Ctrl group.

2.4. Calculation of parameters (Volume, STD, Kurtosis, Skewness)

The methods of evaluation and quality of devices are confirmed and valid by various articles and previous studies in the medical optics field [31-34].

Volume: To calculate the volume of cells using DHM: First, a hologram of the cells is recorded using the DHM setup. This hologram contains the interference pattern of the light wave that has passed through the sample (object wave) and the reference wave.

The recorded hologram is then numerically reconstructed. This involves using algorithms such as the Angular Spectrum Method (The ASP method allows for the reconstruction of the phase and amplitude information of the object, enabling the visualization of three-dimensional structures from a two-dimensional hologram.) to calculate the complex wavefront (amplitude and phase) at the hologram plane.

From the numerically reconstructed wavefront, the phase image is calculated. The phase of the light wave is altered by the cell, depending on the cell's refractive index and thickness. This phase shift is related to the optical path length that the light travels through the cell.

The volume of the cell can be inferred from the phase shift data. As light passes through the cell, the optical path length difference (d(x,y)) is calculated using the Equation 10:

$$\Delta\emptyset = 2\pi/\lambda\,(n-1)\,d(x,y) \quad (10)$$

Where $\Delta\emptyset$ is the phase difference, λ is the wavelength of light, n is the refractive index, and d(x,y) is the physical path difference caused by the cell.

To obtain the volume, an integration of the optical path difference d(x,y) over the area of the cell is performed. This integration sums up all the small volume elements (voxels) that make up the cell.

The actual volume can be calculated using Equation 11:

$$Volume = A.H.n \quad (11)$$

Here, H represents the mean height of the entire cell, A denotes the area of the pixels, and n is the number of pixels.

Standard Deviation (STD): STD is an essential statistical measure that enables quantifying the amount of variation or dispersion within a dataset of height. It is calculated as the square root of the mean of the squared differences from the mean of the set of values (height) (Equation 12).

$$STD = \sqrt{\frac{\sum(h_i - \overline{h})}{n}} \quad (12)$$

Skewness: Spatial skewness, Ssk, the third moment of the deviation, measures the degree of symmetry in roughness about the mean value which heart is the mean height according to Equation 13 Negative skew indicates a predominance of holes, while positive skew indicates a "peaky" surface.

$$Ssk = \frac{1}{Sq^3}\frac{1}{MN}\sum_{i=1}^{M}\sum_{j=1}^{N}[h(x_i,y_j) - \bar{h}(x_i - y_j)]^3 \quad (13)$$

Kurtosis: Spatial kurtosis, Sku, measures the thickness (height) distribution throughout the cell and is related to the width of the distribution according to Equation 14.

$$Sku = \frac{1}{sq^4}\frac{1}{MN}\sum_{i=1}^{M}\sum_{j=1}^{N}[h(x_i,y_j) - \bar{h}(x_i,y_j)]^4 \quad (14)$$

2.5. Statistical Analysis

In this investigation, a minimum of 100,000 MCF7 cells were cultivated within each cellular cohort. Results are presented as Mean ± SD. Statistical comparisons between treatment groups and radiation data were conducted using a t-test implemented through SPSS statistical software, with a predetermined significance level of 95% (P-value less than 0.05).

3. Results

The assessment of morphological parameters serves to elucidate cellular changes subsequent to radiation exposure within the 2 Gy radiation cell group. In Figure 3a, the confluence of MCF7 cells in a 3 cm Petri dish is depicted. Prior to image preprocessing, a greyscale representation was acquired, as illustrated in Figure 3a. Optimal single-cell reconstruction and examination are facilitated by maintaining low confluence and minimizing cell overlap. The reconstructed images, derived from DHM greyscale representations, are portrayed in both Figure 3b and Figure 3c. To ensure representative analysis, Regions Of Interest (ROI) for reconstruction, indicated in yellow, were meticulously chosen from areas of optimal cell density on the culture plate. This selection process was repeated five times across the samples.

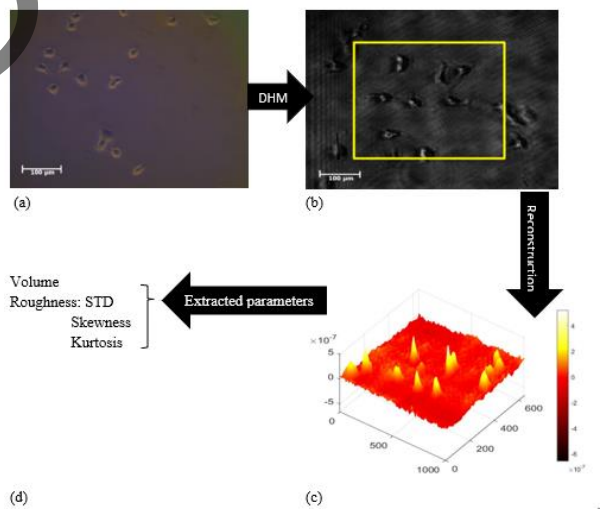

Figure 3. Illustrates the morphological assessment of the Ctrl group through; a) Inverted microscopy image (10X), b) Phase image by DHM, c) Reconstructed Region of Interest (ROI) using MATLAB software, and d) Extraction of volume and roughness parameters of MCF7 cells

A sequence of holographic phase images was employed to evaluate the morphological changes in cells post-radiation. Subsequently, reconstructed images were attained, with the yellow rectangle denoting the Region of Interest (ROI) for which reconstructed images were obtained. In Figure 3a- 3c,

significant noise is observable in the phase plots. This noise arises from the coherent nature of the probe laser radiation and its low intensity, a crucial factor for the non-invasive monitoring of photosensitive cells. However, given that the subsequent determination of cell parameters involved averaging the data over the ROI, this approach substantially mitigated the impact of noise on the obtained results. Figure 4 depicts morphological changes in cell volume and shape within the radiation group (2 Gy).

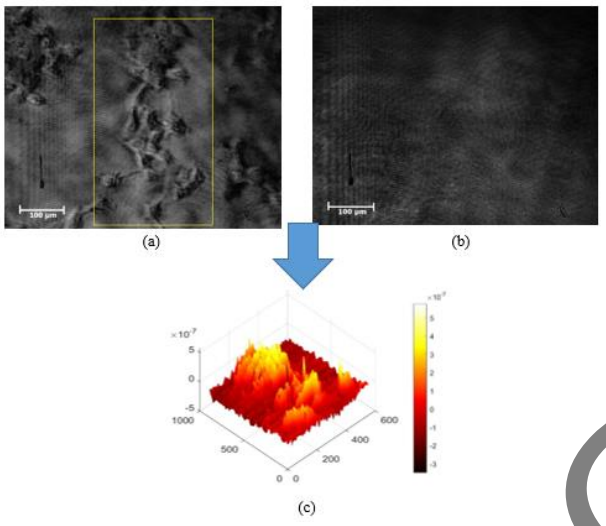

Figure 4. Representation of MCF7 cells post-radiation (Radiation): a) DHM image (yellow rectangle indicates Region of Interest [ROI]); b) Reference image; c) Reconstruction of ROI

It has been observed through studies that radiation can instigate diverse morphological alterations in MCF7 cells, encompassing changes in cell shape, size, and roughness. To scrutinize these morphological transformations, parameters such as volume, STD, kurtosis, and skewness were extracted during the reconstruction process. In Figure 5, these four parameters are presented as the ratio of the corresponding Radiation parameter to the Ctrl parameter.

The volume, STD, kurtosis, and skewness of cell images in the radiation group exhibited a significant increase, surpassing those in the Ctrl group by factors of 2.90, 0.94, 1.26, and 1.30, respectively, following exposure to 2 Gy radiation. This augmentation in holographic image parameters within the radiation group, in contrast to the Ctrl group, suggests a potential correlation with the administered radiation dose, energy transfer, and resultant cellular damage.

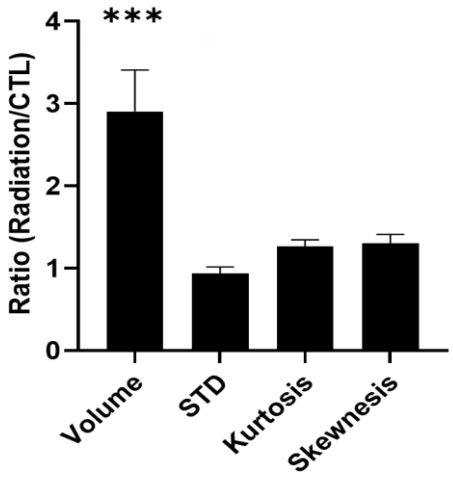

Figure 5. Comparative analysis of morphological changes in radiation-exposed MCF7 cells versus Ctrl cells using parameters (Volume, STD, Skewness, Kurtosis) derived from the 3D reconstruction of DHM images

4. Discussion

These investigations underscore the potential of DHM for examining the impact of radiation on MCF7 cells at a cellular level. The alterations in the morphology of breast cancer cells following radiation therapy offer a novel perspective, effectively delineating the consequences of radiotherapy radiation or high-energy ionizing radiation on cellular structures. The results unequivocally demonstrate that radiation can elicit diverse morphological changes in MCF7 cells, including alterations in cell shape. In Figure 3, the extraction of image parameters from a single cell is depicted. Figure 3a indicates cases of the initial state of seeded cells in 3 cm Petri dishes before x-ray radiation, captured by an inverted microscope. The microscopic portrayal of MCF7 cells, illustrating cell confluence for the examination of morphological characteristics, is presented in Figure 3b. The image is subsequently reconstructed. DHM proves instrumental in quantifying changes in volume, STD, kurtosis, and skewness. This technique provides a valuable means to explore the underlying mechanisms through which radiation influences the morphology and behavior of cancer cells.

MCF7 cells exhibit sensitivity to ionizing radiation, potentially inducing damage and leading to cell death. DHM has been leveraged to scrutinize the effects of radiation on MCF7 cells, allowing for the real-time

monitoring of changes in cell morphology and behavior. Figure 3 underscores that MCF7 cells exposed to low doses of radiation undergo discernible changes in cell shape. Figure 5 presents the parameters derived from the reconstruction of holographic images, illustrating distinctions between Ctrl and radiation-exposed groups. Notably, the results underscore variations in cell volume between the Ctrl and radiation groups. This study demonstrates the feasibility of quantitatively assessing the volume of viable cells cultured in containers using a holographic microscope. Previously, in the study of Aidan *et al.*, using DHM, various and valuable morphological features such as texture cluster shade were identified and introduced to identify the MCF7 (breast cancer cells) cell line compared to the MCF10A (normal breast cells) cell line [31]. In another study, biomechanical properties of invasive (MDA-MB-231) and non-invasive (MCF-7) breast cancer cell lines were investigated using digital holographic microscopy. The results showed a higher strain in the invasive cell lines, which is due to the metastatic nature of these cells [32]. Pirone *et al.* used holographic digital flow cytometry to collect images of flowing cells. After extracting the scores of significant morphometric features, it was found that 3D morphological features have higher accuracy in classifying and identifying drug-resistant endometrial cancer cells [33].

In addition, recent studies have focused on the classification of elliptical cancer cells using DHM imaging and morphological data. For this purpose, different methods such as deep image learning based on a CNN design or modern deep-image learning technique, self-supervised learning have been used [34, 35]. The volumetric parameter, denoting the three-dimensional (3D) volume of the reconstructed object from a hologram, assumes significance in DHM. This parameter serves as a pivotal quantitative metric enabling the characterization of size, shape, and morphology in biological cells, tissues, and other specimens. Precise volume measurements furnish researchers with information about physical properties such as density, mass, and surface area, facilitating the investigation of diverse biological processes and phenomena. Furthermore, the volumetric parameter allows for comparisons between different samples or conditions and the monitoring of temporal changes in size or shape. In recent years, numerous studies have explored the impact of chemical and physical interventions on cell morphology using DHM. For instance, Kemper *et al.* (2006) utilized a DH microscope to investigate the initial effects of the drug Latrunculin B on the morphological changes in pancreatic cancer cells [17]. Similarly, El-Schich *et al.* (2015) observed an increase in the volume of prostate cancer cells treated with the chemotherapy drug "etoposide" [36]. However, research on describing and investigating morphological changes in cancer cells post-radiation remains limited, with no specific and significant factors or parameters introduced thus far. Notably, a recent study by Xiao *et al.* (2022) highlighted the potential of using morphological characteristics to estimate the radiosensitivity of bladder cancer cells, proposing the application of DH microscopes for detecting radiosensitivity and guiding radiation therapy in bladder cancer [10].

Concurrently, kurtosis serves as another extracted parameter in DHM. A marked increase in the kurtosis of irradiated cells compared to the Ctrl group has been discerned. In DHM, kurtosis is a statistical measure employed to quantify the deviation of the intensity distribution of a hologram from a normal distribution. It gauges the "tailedness" of the intensity distribution, signifying the extent to which it diverges from a normal (Gaussian) distribution. A high kurtosis value denotes that the distribution harbors more extreme values (outliers) than a normal distribution, while a low kurtosis value suggests fewer extreme values. In the context of DHM, kurtosis serves as a diagnostic tool to recognize and quantify aberrations within the optical setup or the sample itself, influencing the hologram's quality and the precision of the reconstructed image. Researchers can evaluate hologram quality and identify potential errors in the DHM setup by measuring kurtosis and comparing it to the expected value for a normal distribution.

Corroborating these findings, Dubey's (2019) study also reveals an increase in kurtosis (2.469) and skewness (0.775) in the treated group and 2.197 and 0.669 in the Ctrl group, respectively. These outcomes indicate increased flatness and asymmetry after exposure to 10µMol H_2O_2 in the treated group [23]. Similarly, a noteworthy elevation in the irradiated group was observed during the examination of MCF7 skewness parameters. In DHM, skewness, another statistical measure, quantifies the degree of asymmetry in the intensity distribution of a hologram. It signifies the extent to which the distribution deviates from symmetry relative to a normal (Gaussian) distribution. A positive skewness value suggests a longer tail to the right in the

distribution (more high-intensity values), while a negative skewness value implies a longer tail to the left (more low-intensity values). Skewness in DHM serves as a valuable metric to pinpoint and measure aberrations in the optical setup or the sample, impacting hologram quality and reconstructed image accuracy. Researchers can evaluate hologram quality and identify potential errors in the DHM setup by measuring skewness and comparing it to the anticipated value for a normal distribution.

Furthermore, the radiation group exhibits a lower STD, indicating a reduced spread of data points around the mean value. STD in the intensity distribution serves as a metric for gauging the degree of variation in intensity values across the hologram. A heightened STD value suggests a more dispersed arrangement of intensity values, while a diminished STD value signifies a more closely clustered distribution around the mean. Within the realm of DHM, STD assumes significance in evaluating hologram quality and the signal-to-noise ratio of the reconstructed image. An elevated STD value implies a hologram with more noise and less signal, whereas a lower STD value suggests a hologram with less noise and more signal. Researchers, through STD measurement of the hologram, can fine-tune DHM setup and processing parameters to enhance image quality and the precision of the reconstructed image. As evidenced by Dubey's (2019) study, the evaluated STD was 0.857 in contrast to 0.965 in the Ctrl group [23].

DHM was employed to quantitatively assess radiation-induced alterations in MCF7 cell morphology, encompassing changes in cell volume, surface area, and aspect ratio. Significantly, radiation elicited pronounced changes in all these parameters, establishing them as potential quantitative biomarkers of radiation response. The study underscores radiation's capability to impact cancer cell volume, thereby inducing substantial morphological transformations. Notably, discernible alterations in cell morphology were observed 24 hours post-irradiation, as depicted in Figure 4 where radiation led to an increase in cell volume. A congruent study by Kawase *et al.* similarly documented heightened volume in cells under gamma ionizing radiation influence [37]. Despite their potential significance, studies of this nature have received comparatively less attention, partly attributed to challenges in determining cell volume without enzymatic or mechanical separation [37, 38].

The DH microscope's unique parameters render it particularly suitable for this investigation. Key advantages include its capacity to furnish quantitative insights into cell structure, obviating the need for intricate preparation procedures such as cell labeling, enabling parallel use of cells for other methods without compromising cell integrity, and facilitating high-speed, automated, and non-invasive processes. The study's results reveal substantial morphological distinctions between irradiated and Ctrl group cells. Our observation has limitations. First, only the MCF7 cell line was used in this study, and the findings may not be generalizable to other breast cancer cell lines. Second, we did not observe a specific morphological parameter associated with irradiation and the deformation was non-specific. Third, it is better to perform molecular or genetic analysis to validate the results.

5. Conclusion

DHM emerges as a potent tool for qualitative examination of morphological shifts in MCF7 cells pre- and post-radiation. This research offers valuable perspectives into radiation's impact on cancer cells at the cellular level, holding implications for the development of novel treatments or strategies to enhance the efficacy of existing therapies.

Acknowledgements

Thanks to Iran University of Medical Sciences for their help and support. There is no conflict of interest.

References

1- Gomathi Mohan, Ayisha Hamna T P, Jijo A J, Saradha Devi K M, Arul Narayanasamy, and Balachandar Vellingiri, "Recent advances in radiotherapy and its associated side effects in cancer—a review." *The Journal of Basic and Applied Zoology*, Vol. 80 (No. 1), p. 14, 2019/02/27 (2019).

2- R. A. Chandra, F. K. Keane, F. E. M. Voncken, and C. R. Thomas, Jr., "Contemporary radiotherapy: present and future." (in eng), *Lancet*, Vol. 398 (No. 10295), pp. 171-84, Jul 10 (2021).

3- S. K. Vinod and E. Hau, "Radiotherapy treatment for lung cancer: Current status and future directions." (in eng), *Respirology*, Vol. 25 Suppl 2pp. 61-71, Nov (2020).

4- M. Baumann *et al.*, "Radiation oncology in the era of precision medicine." (in eng), *Nat Rev Cancer,* Vol. 16 (No. 4), pp. 234-49, Apr (2016).

5- A. I. Goranov *et al.*, "Changes in cell morphology are coordinated with cell growth through the TORC1 pathway." (in eng), *Curr Biol,* Vol. 23 (No. 14), pp. 1269-79, Jul 22 (2013).

6- B. R. Hughes, M. Mirbagheri, S. D. Waldman, and D. K. Hwang, "Direct cell-cell communication with three-dimensional cell morphology on wrinkled microposts." (in eng), *Acta Biomater,* Vol. 78pp. 89-97, Sep 15 (2018).

7- I. Nassiri and M. N. McCall, "Systematic exploration of cell morphological phenotypes associated with a transcriptomic query." (in eng), *Nucleic Acids Res,* Vol. 46 (No. 19), p. e116, Nov 2 (2018).

8- S. Tatapudy, F. Aloisio, D. Barber, and T. Nystul, "Cell fate decisions: emerging roles for metabolic signals and cell morphology." (in eng), *EMBO Rep,* Vol. 18 (No. 12), pp. 2105-18, Dec (2017).

9- S. A. Narayanan, J. Ford, and D. C. Zawieja, "Impairment of lymphatic endothelial barrier function by X-ray irradiation." (in eng), *Int J Radiat Biol,* Vol. 95 (No. 5), pp. 562-70, May (2019).

10- Xi Xiao *et al.*, "Label-free observation of morphological alteration of irradiated-urothelial bladder carcinoma cells through digital holographic microscopy." *Frontiers in Physics,* Vol. 10p. 925523, August 01, 2022 (2022).

11- M. Rubin *et al.*, "TOP-GAN: Stain-free cancer cell classification using deep learning with a small training set." (in eng), *Med Image Anal,* Vol. 57pp. 176-85, Oct (2019).

12- Bahram Javidi *et al.*, "Roadmap on digital holography [Invited]." *Optics Express,* Vol. 29 (No. 22), pp. 35078-118, 2021/10/25 (2021).

13- D. Carl, B. Kemper, G. Wernicke, and G. von Bally, "Parameter-optimized digital holographic microscope for high-resolution living-cell analysis." (in eng), *Appl Opt,* Vol. 43 (No. 36), pp. 6536-44, Dec 20 (2004).

14- K. J. Chalut, A. E. Ekpenyong, W. L. Clegg, I. C. Melhuish, and J. Guck, "Quantifying cellular differentiation by physical phenotype using digital holographic microscopy." (in eng), *Integr Biol (Camb),* Vol. 4 (No. 3), pp. 280-4, Mar (2012).

15- F. Charrière *et al.*, "Living specimen tomography by digital holographic microscopy: morphometry of testate amoeba." (in eng), *Opt Express,* Vol. 14 (No. 16), pp. 7005-13, Aug 7 (2006).

16- Pietro Ferraro *et al.*, "Extended focused image in microscopy by digital Holography." *Optics Express,* Vol. 13pp. 6738-49, 10/01 (2005).

17- B. Kemper *et al.*, "Investigation of living pancreas tumor cells by digital holographic microscopy." (in eng), *J Biomed Opt,* Vol. 11 (No. 3), p. 34005, May-Jun (2006).

18- Benjamin Rappaz, Pierre Marquet, Etienne Cuche, Yves Emery, Christian Depeursinge, and Pierre J. Magistretti, "Measurement of the integral refractive index and dynamic cell morphometry of living cells with digital holographic microscopy." *Optics Express,* Vol. 13 (No. 23), pp. 9361-73, 2005/11/14 (2005).

19- Christopher J. Mann, Lingfeng Yu, Chun-Min Lo, and Myung K. Kim, "High-resolution quantitative phase-contrast microscopy by digital holography." *Optics Express,* Vol. 13 (No. 22), pp. 8693-98, 2005/10/31 (2005).

20- Myung- K. Kim, "Applications of Digital Holography in Biomedical Microscopy." *Journal of the Optical Society of Korea,* Vol. 14 (No. 2), pp. 77-89, 2010/06/25 (2010).

21- Georges Nehmetallah and Partha P. Banerjee, "Applications of digital and analog holography in three-dimensional imaging." *Advances in Optics and Photonics,* Vol. 4 (No. 4), pp. 472-553, 2012/12/31 (2012).

22- Yunxin Wang *et al.*, "Morphological Measurement of Living Cells in Methanol with Digital Holographic Microscopy." *Computational and Mathematical Methods in Medicine,* Vol. 2013p. 715843, 2013/01/27 (2013).

23- Vishesh Dubey *et al.*, "Partially spatially coherent digital holographic microscopy and machine learning for quantitative analysis of human spermatozoa under oxidative stress condition." *Scientific Reports,* Vol. 9 (No. 1), p. 3564, 2019/03/05 (2019).

24- Kendra L. Barker, Kenneth M. Boucher, and Robert L. Judson-Torres, "Label-Free Classification of Apoptosis, Ferroptosis and Necroptosis Using Digital Holographic Cytometry." *Applied Sciences,* Vol. 10 (No. 13), p. 4439, (2020).

25- Joost Verduijn, Louis Van der Meeren, Dmitri V. Krysko, and André G. Skirtach, "Deep learning with digital holographic microscopy discriminates apoptosis and necroptosis." *Cell Death Discovery,* Vol. 7 (No. 1), p. 229, 2021/09/02 (2021).

26- Tomas Vicar, Martina Raudenska, Jaromir Gumulec, and Jan Balvan, "The Quantitative-Phase Dynamics of Apoptosis and Lytic Cell Death." *Scientific Reports,* Vol. 10 (No. 1), p. 1566, 2020/01/31 (2020).

27- AA Zhikhoreva *et al.*, "Significant difference in response of malignant tumor cells of individual patients to photodynamic treatment as revealed by digital holographic microscopy." *Journal of Photochemistry and Photobiology B: Biology,* Vol. 221p. 112235, (2021).

28- Maria Baczewska *et al.*, "Method to analyze effects of low-level laser therapy on biological cells with a digital holographic microscope." *Applied Optics,* Vol. 61 (No. 5), pp. B297-B306, (2022).

29- Yakun Liu, Leiping Che, Hui Zhao, Yijing Li, Wen Xiao, and Feng Pan, "Observing the Morphological Changes of Irradiated Bladder Carcinoma Cells Using Digital Holographic Microscopy." in *Applied Industrial*

Spectroscopy, (2021): *Optica Publishing Group*, p. JTu5A. 33.

30- J.W. Goodman, Introduction to Fourier Optics. *W. H. Freeman*, (2005).

31- Aidan J McLaughlin, Anthony J Kaniski, Darena I Matti, and Besa Xhabija, "Comparative Morphological Analysis of MCF10A and MCF7 Cells Using Holographic Time-lapse Microscopy." *Anticancer Research*, Vol. 43 (No. 9), pp. 3891-96, (2023).

32- Hasan Berkay Abdioglu *et al.*, "Biomechanical Analysis Of Breast Cancer Cells: A Comparative Study Of Invasive And Non-Invasive Cell Lines Using Digital Holographic Microscopy." *arXiv e-prints*, p. arXiv: 2311.12739, (2023).

33- Daniele Pirone *et al.*, "Identification of drug-resistant cancer cells in flow cytometry combining 3D holographic tomography with machine learning." *Sensors and Actuators B: Chemical*, Vol. 375p. 132963, (2023).

34- Kevyan Jaferzadeh, Seungwoo Son, Abdur Rehman, Seonghwan Park, and Inkyu Moon, "Automated Stain-Free Holographic Image-Based Phenotypic Classification of Elliptical Cancer Cells." *Advanced Photonics Research*, Vol. 4 (No. 1), p. 2200043, (2023).

35- Abdur Rehman, Hyunbin An, Seonghwan Park, and Inkyu Moon, "Automated classification of elliptical cancer cells with stain-free holographic imaging and self-supervised learning." *Optics & Laser Technology*, Vol. 174p. 110646, (2024).

36- Z. El-Schich, A. Mölder, H. Tassidis, P. Härkönen, M. Falck Miniotis, and A. Gjörloff Wingren, "Induction of morphological changes in death-induced cancer cells monitored by holographic microscopy." (in eng), *J Struct Biol*, Vol. 189 (No. 3), pp. 207-12, Mar (2015).

37- T. Kawase, K. Okuda, M. Nagata, M. Tsuchimochi, H. Yoshie, and K. Nakata, "Non-invasive, quantitative assessment of the morphology of γ-irradiated human mesenchymal stem cells and periosteal cells using digital holographic microscopy." (in eng), *Int J Radiat Biol*, Vol. 92 (No. 12), pp. 796-805, Dec (2016).

38- T. Kawase *et al.*, "Evaluating the Safety of Somatic Periosteal Cells by Flow-Cytometric Analysis Monitoring the History of DNA Damage." (in eng), *Biopreserv Biobank*, Vol. 14 (No. 2), pp. 129-37, Apr (2016).